



Published in final edited form as:

Biomaterials. 2016 January ; 77: 280–290. doi:10.1016/j.biomaterials.2015.10.045.

Spatially localized recruitment of anti-inflammatory monocytes by SDF-1 α -releasing hydrogels enhances microvascular network remodeling

JR Krieger^{1,*}, ME Ogle^{1,*}, J McFaline-Figueroa¹, CE Segar¹, JS Temenoff^{1,2}, and EA Botchwey^{1,2}

¹W.H. Coulter Department of Biomedical Engineering, Georgia Institute of Technology and Emory University, Atlanta, GA 30332, USA

²Petit Institute for Bioengineering and Bioscience, Georgia Institute of Technology, Atlanta, GA, 30332, USA

Abstract

Tissue repair processes are characterized by the biphasic recruitment of distinct subpopulations of blood monocytes, including classical (“inflammatory”) monocytes (IMs, Ly6C^{hi}Gr1⁺CX3CR1^{lo}) and non-classical anti-inflammatory monocytes (AMs, Ly6C^{lo}Gr1⁻CX3CR1^{hi}). Drug eluting biomaterial implants can be used to tune the endogenous repair process by the preferential recruitment of pro-regenerative cells. To enhance recruitment of AMs during inflammatory injury, a novel N-desulfated heparin-containing poly(ethylene glycol) diacrylate (PEG-DA) hydrogel was engineered to deliver exogenous stromal derived factor-1 α (SDF-1 α), utilizing the natural capacity of heparin to sequester and release growth factors. SDF-1 α released from the hydrogels maintained its bioactivity and stimulated chemotaxis of bone marrow cells *in vitro*. Intravital microscopy and flow cytometry demonstrated that SDF-1 α hydrogels implanted in a murine dorsal skinfold window chamber promoted spatially-localized recruitment of AMs relative to unloaded internal control hydrogels. SDF-1 α delivery stimulated arteriolar remodeling that was correlated with AM enrichment in the injury niche. SDF-1 α , but not unloaded control hydrogels, supported sustained arteriogenesis and microvascular network growth through 7 days. The recruitment of AMs correlated with parameters of vascular remodeling suggesting that tuning the innate immune response by biomaterial SDF-1 α release is a promising strategy for promoting vascular remodeling in a spatially controlled manner.

Keywords

Vascularization; immunomodulation; angiogenesis; arteriogenesis; SDF-1; hydrogel

Corresponding Author: Edward Botchwey, Department of Biomedical Engineering, Georgia Institute of Technology, 315 Ferst Drive, Atlanta, Ga 30332, edward.botchwey@bme.gatech.edu, Phone: (404) 385-5058, Fax: (404) 894-4243.

*These authors contributed equally to this work.

Publisher's Disclaimer: This is a PDF file of an unedited manuscript that has been accepted for publication. As a service to our customers we are providing this early version of the manuscript. The manuscript will undergo copyediting, typesetting, and review of the resulting proof before it is published in its final citable form. Please note that during the production process errors may be discovered which could affect the content, and all legal disclaimers that apply to the journal pertain.

Introduction

Monocytes are a heterogeneous population of cells that are dynamically recruited to damaged tissues to support injury repair, tissue remodeling, and regeneration [1-5]. Circulating blood monocytes are found in at least two phenotypic states, the classical “inflammatory” and the non-classical “anti-inflammatory” monocyte. Inflammatory monocytes (IMs), CD45⁺CD11b⁺Ly6C^{hi}Gr1⁺CX3CR1^{low} in mice and CD14⁺CD16⁻ monocytes in humans, are mobilized from bone marrow (BM) and spleen in response to injury and subsequently recruited to sites of inflammation to expand peripheral mononuclear phagocytes [6, 7]. Anti-inflammatory monocytes (AMs), CD45⁺CD11b⁺Ly6C^{low}Gr1⁻CX3CR1^{high} in mice and CD14^{low}CD16⁺ monocytes in humans, patrol the luminal side of endothelium at steady state and are associated with pro-regenerative activities [8]. Implications for understanding the division of labor among monocyte subpopulations and their progeny during tissue repair are far-reaching. Injuries such as myocardial infarct produce coordinated chemokine expression profiles to recruit and position IMs and AMs sequentially, exploiting the phagocytic and proteolytic activities of IMs in early stages post-infarct and the anti-inflammatory/pro-angiogenic properties of AMs in later healing stages [9-11]. Key regulatory roles for functionally distinct monocyte subsets and their progeny have been described in numerous other models including bone formation [5, 12], spinal cord injury healing [13, 14], limb regrowth [15], pathogen clearance, embryonic development, and tissue homeostasis [16]. A further understanding of the mechanisms regulating the kinetics and activities of these two monocyte populations during normal wound healing will advance therapeutic targeting of desired cells and regulation of the “injury niche” to support their function within regenerating tissue.

Formation of stable vascular networks during wound repair supplies oxygen and nutrients required for regeneration or biomaterial/tissue implant integration. Vascular remodeling occurs through the complementary processes of angiogenesis (growth of new vessels from existing vascular network) and arteriogenesis (structural expansion of arteriolar conduits to allow increased perfusion). Recruitment and retention of leukocytes by soluble chemotactic gradients within the injury niche is a key determinant of microvascular growth and remodeling [17-20]. Notably, the perivascular positioning of monocytes is a hallmark of the angiogenic program induced by growth factors such as vascular endothelial growth factor (VEGF) [21]. Stromal derived factor-1 α (SDF-1 α) is a CXC family chemokine that is increased in tissue after injury and mediates the recruitment of innate immune cells that directly and indirectly participate in the growth of microvascular networks. SDF-1 α signals through its cognate G-protein coupled receptor CXC chemokine receptor type 4 (CXCR4), which is highly expressed on immune cells and several known adult stem/progenitor cell sources, including mesenchymal stem cells, hematopoietic stem cells, and endothelial progenitor cells among others [22-24]. Previous reports suggest a prominent role for the cell surface receptor CXCR4 in regulating monocyte retention and tissue distribution following tissue damage [20, 25, 26]. We have also observed that AMs in particular may be functionally distinguished from IMs by their increased CXCR4-mediated chemotaxis and that selective recruitment of AMs along peri-implant arterioles promotes growth and maturation of microvessel networks in both skin and muscle injury models [17, 19].

In this study, we investigate how localized presentation of SDF-1 α from engineered hydrogels impacts the recruitment and strategic distribution of circulating monocytes populations during sterile inflammatory wound healing and vascular remodeling. We have shown previously that particular derivatives of the glycosaminoglycan (GAG) heparin can protect growth factors such as BMP-2 from denaturing conditions, and that heparin-based biomaterials enable sustained presentation of biomolecular cargo and decrease the amount of growth factor necessary to achieve the same physiological response as bolus delivery [27-29]. Heparin enhances the loading of growth factor cargo into biomaterials and increased heparin content in the material can enhance the amount of growth factor released, likely by preventing denaturation of the growth factor within the carrier [29]. Thus, heparin derivatives are an excellent choice for sustained delivery of heparin-binding proteins such as SDF-1 α [30]. To enable safe *in vivo* use of heparin-based biomaterials in present and future studies, we employed a desulfated heparin formulation that exhibits very low anticoagulant activity and extends the half-life of growth factors in solution and in delivery systems [28, 29, 31-36]. In this study, hydrogel matrices were fabricated by cross-linking N-desulfated heparin methacrylamide and poly(ethylene glycol) diacrylate (PEG-DA) (hereafter called Hep^N hydrogels) and loaded with recombinant murine SDF-1 α in the presence of albumin as an additional stabilizing factor [37, 38]. Release of SDF-1 α from Hep^N hydrogels was sustained over at least 3 days *in vitro* and retained the ability to induce chemotaxis of primary bone marrow-derived cells. The murine dorsal skinfold window chamber, a model of inflammatory vascular remodeling, was utilized to longitudinally test the *in vivo* effects of affinity-based delivery of SDF-1 α on recruitment of circulating monocytes and associated microvascular network regeneration and expansion. SDF-1 α -loaded Hep^N hydrogels were co-implanted in the dorsal skin window chamber with internal control hydrogels not containing SDF-1 α . Multiple types of analysis, including intra-vital microscopy, flow cytometry, and whole-mount immunostaining of dorsal skin tissues show that SDF-1 α presentation from Hep^N hydrogels results in highly localized recruitment of bone marrow-derived monocytes (predominantly AMs) to the injury niche without significantly altering the distribution of cells adhered at the hydrogel implant and tissue interface. SDF-1 α -induced recruitment of host cells significantly increased the caliber and number of perihydrogel microvessels versus internal controls, suggesting an exciting potential of the growth factor-releasing Hep^N hydrogel technology to locally tune the interaction of innate immune cell populations with the injury niche to promote regeneration.

Materials and Methods

Heparin chemical modification

Heparin sodium salt (Sigma) was reconstituted with distilled, deionized water (ddH₂O) at 10mg/mL and desalted using Dowex 50WX4 resin (mesh size 100-200, Sigma), adding pyridine until the pH reached a value of ~6, as previously described [28]. The solution was reduced and excess pyridine was eliminated using a rotary evaporator (Buchi) before being flash frozen and lyophilized to yield heparin pyridinium salts. The heparin pyridinium salts were then dissolved in solution of 90% DMSO/10% ddH₂O (v/v) at a concentration of 1mg/mL. The solution was mixed for 2h at 50°C in a rotary evaporator and then cooled on ice and precipitated by an equal volume of 95% ethanol (VWR) saturated with sodium

acetate (VWR). The precipitate was centrifuged and washed with ethanol prior to dissolving in distilled water (dH₂O). The solution was dialyzed for 3 days with daily exchanges of dH₂O and then lyophilized (Labconco). Finally, the product was functionalized using a 8.0 molar excess of N-(3-aminopropyl) methacrylamide hydrochloride (APMam, Polysciences), N-hydroxysuccinimide (NHS, Acros Organics) and N-3-dimethylaminopropyl)-N'-ethylcarbodiimide hydrochloride (EDC, Sigma) at an acidic pH. After functionalization, the solution was dialyzed and lyophilized again as described previously. The finished product was stored at -20°C until use.

PEG-DA synthesis

Distilled methylene chloride (DCM) was used to dissolve 3.4 kDa PEG in a three neck round-bottom flask and stirred under nitrogen flow. First, triethylamine in DCM at a 1:1 molar ratio with the PEG was added. Subsequently, a 100% molar excess of acryloyl chloride (AcCl) in 15-20mL of DCM was added dropwise. Following the AcCl addition, the system was closed and kept under nitrogen overnight. Potassium carbonate (K₂CO₃) was then added to the solution to remove trimethylamine hydrochloride by-product created in the previous step. After separation of the organic phase, the PEG-DA was precipitated using cold diethyl ether and dried overnight at RT. The finished product was stored at -20°C until use.

Hydrogel fabrication

PEG-DA and N-desulfated heparin (Hep^N) were used as a mixture of 90:10 by weight in all hydrogels. These polymers were UV sterilized and combined at a 10 wt% total solution ratio with sterile phosphate buffered saline (PBS), thermal initiators ammonium persulfate (APS, 0.018M, Sigma) and N,N,N',N'-tetramethylethane-1,2-diamine (TEMED, 0.018M, Sigma), and an amount of GMP-quality bovine serum albumin (BSA, Sigma #A8412) equivalent to 50 wt% of the solution. The solution was then pipetted between two sterile glass slides with an inner clearance of 500µm. The solution was allowed to gel at 37°C for 10 min before the gels were punched out using a 2mm (diameter) biopsy punch (Miltex). The resulting hydrogels were discs of 0.5mm thickness and 2mm diameter.

NMR Analysis of heparin and PEG-DA polymers

Proton nuclear magnetic resonance (¹H NMR) was used to characterize the polymers used for hydrogel fabrication (Figure S1). Samples of N-desulfated heparin methacrylamide (Hep^N Mam) and poly(ethylene glycol) diacrylate (PEG-DA) were diluted to a concentration of 10 mg/mL with deuterated water (D₂O) and ¹H NMR was measured on a Bruker Avance III 400 spectrometer at 400 MHz. To determine the degree of functionalization of the Hep^N MAM derivative, first the contributions of N-acetyl protons in un-functionalized specimens were determined (Figure S1A). Subsequently, the ratio of protons donated by methacrylate groups was multiplied by the native N-acetyl groups from unfunctionalized samples (Figure S1B). The contribution of native methyl groups in non-methacrylated material was approximately 8-9%. The degree of functionalization in Hep^N MAM was ~20% for the *in vitro* assays in Figure S2. For the characterization of PEG-DA, the presence of acrylate peaks around 5.8-6.4 ppm were observed (Figure S1C).

SDF-1 α loading and in vitro release

Gels were placed in ultra-low binding 24-well plates and rinsed with PBS for 3h prior to loading with recombinant murine SDF-1 α (Peprotech) overnight at 4°C. During this time, each gel was incubated with a 10 μ L droplet of PBS containing 0.1 μ g growth factor or no protein (control gels). After loading, the wells were filled with 500 μ L of PBS and incubated at 37°C for the release study. PBS was exchanged at appropriate timepoints and stored at -20°C for subsequent analysis.

In vitro migration

SDF-1 α loaded gels (aHep^N-SDF) or albumin loaded control gels (aHep^N) were incubated with 650 μ L of Iscove's Modified Dulbecco's Medium (Fisher) containing 0.5% fatty acid-free bovine serum albumin (Fisher) for 24h at 37°C. A transwell assay was assembled by transferring hydrogel-conditioned media to the chamber below a 5 μ m pore size membrane, and seeding 4 \times 10⁵ cells from C57BL/6 mouse bone marrow aspirate on top. After 4h of migration at 37°C and 5% CO₂, migrated cells were stained with DRAQ5 dye according to manufacturer's protocol (Cell Signaling Technologies). Relative migration was quantified by fluorescence intensity using an Odyssey CLx Infrared Imaging System (LI-COR Biosciences).

Chimeric mice

All animal procedures were conducted according to protocols approved by the Georgia Tech Institutional Animal Care and Use Committee. For generation of mice with chimeric EGFP-labeled bone marrow, male C57BL/6 recipient mice, 8-10 weeks of age, were lethally irradiated with a total dosage of 10.5 Gy (5.5-Gy and 5-Gy doses, 3h apart) using an x-ray source (Radsources 2000). Animals were given water supplemented with Baytril for 1 week before and 2 weeks after irradiation and bone marrow cell transplantation. Transplants were performed by injecting 1 \times 10⁷ bone marrow cells harvested from transgenic EGFP (donor) mice into the jugular vein of recipient mice under inhaled isoflurane anesthesia. Mice were allowed to recover for at least 4 weeks prior to surgery.

Dorsal skinfold window chamber

Male C57BL/6 mice aged 8-12 weeks of age were anesthetized by i.p. injection of a mixture of ketamine (100mg/kg) and xylazine (10mg/kg) in sterile 0.9% saline and surgically fitted with sterile dorsal skinfold window chambers (APJ Trading Co.) as previously described [17, 19, 39, 40]. Briefly, dorsal skin was shaved, depilated, and sterilized via triplet washes of 70% ethanol and chlorhexidine. A double-layered skin fold was elevated off the back of the mouse and the back side of the titanium window chamber frame was surgically fixed to the underside of the skinfold. Surgical microscissors were used to remove the epidermis and dermis from the top-side of the skinfold in a circular area (diameter = 12mm) to reveal the vasculature underlying the reticular dermis. Exposed tissue was kept hydrated with sterile saline. The front side of the titanium frame was then mounted on the top of the dissected tissue and attached to its underlying counterpart. The dorsal skin was sutured to the two titanium frames, and the exposed tissue was sealed with a protective sterile glass coverslip. Mice were allowed to recover in heated cages and administered sustained release

buprenorphine via i.p. injection as a postoperative analgesic. All mice received a laboratory diet and water *ad libitum* throughout the course of the experiment.

Hydrogel placement and intravital brightfield microscopy

Hydrogels were implanted into the window chamber on the day of surgery (day 0). Mice were anesthetized via inhaled isoflurane, the glass window was removed and dorsal tissue was flooded with 1mM adenosine in Ringer's solution to maximally dilate all vessels and maintain tissue hydration. The mouse was then mounted to a custom microscope stage mount and imaged noninvasively at 5× magnification on a Zeiss Imager.D2 microscope with AxioCam MRc 5 color digital camera (Carl Zeiss). Images were acquired on day 0 immediately preceding hydrogel implantation and again on day 3 or 7 according to experimental design. Mice were implanted with one Hep^{-N} internal control hydrogel and one aHep^{-N} experimental hydrogel (unloaded or loaded with SDF-1α) placed on opposite sides of the window.

Changes in microvascular length density

Microvascular length density measurements were made by intravital brightfield microscopy and whole mount immunofluorescence. A 4mm (diameter) region of interest circumscribing the hydrogel and tangential to the gel edge was selected as indicated in Figure S4. Vessels visible within these cropped images were traced and total vessel length per unit area was quantified using ImageJ.

Measurement of change in arteriolar diameter

To measure changes in arteriolar diameter, arteriole–venule pairs were identified within a 3mm radius of the center of each gel. Arterioles and venules were identified on the basis of size and morphology at day 0; venular diameters were larger than arteriolar diameters on day 0. Internal diameters based on blood column width in brightfield images were measured using Zen Blue (Zeiss) and recorded longitudinally for each vessel segments on day 0 and 3 or day 0 and 7 (Figure S3). Day 0 diameter measurements were used to bin vessels less than 40μm in diameter [41]. This metric is limited to vessels visible at both time points (1–4 vessels/gel).

Hydrogel removal, tissue harvest, and preparation for single-cell suspensions

To visualize the recruitment of cells to the hydrogel interface, hydrogels were explanted onto glass slides and imaged at 5× magnification. For subsequent flow cytometry analysis, cells were then removed from the hydrogel surface by incubation with trypsin for 10min at 37°C and combined with a fixed volume of flow cytometry counting beads for quantification of relative cell number, CountBright™ Absolute Counting Beads (Life Technologies). To measure the recruitment of cells to tissue by day 3, the dorsal tissue was bisected along the midline separating the hydrogels, digested with 1mg/mL collagenase at 37°C, and further disaggregated with a cell strainer to create a single cell suspension.

Flow cytometry

Immuno-staining and flow cytometry analyses were performed according to standard procedures and analyzed on a FACS-AriaIIIu flow cytometer (BD Biosciences). The following antibodies were used for cell phenotyping: APC/Cy7-conjugated anti-CD11b (BioLegend, M1/70), APC-conjugated anti-Ly-6C (BioLegend, HK1.4), and PE- or PerCP/Cy5.5-conjugated anti-CXCR4 (eBiosciences, 2B11). CD11b⁺SSC^{low}Ly-6C^{high/low} monocyte populations were confirmed to be Ly-6G^{neg}.

Whole mount immunohistochemistry and intravital confocal microscopy

Mouse vasculature was perfused with warm 0.9% saline and then 4% PFA until tissues were fixed. Dorsal tissue was explanted and drop-fixed in 4% PFA for 10min, permeabilized with 0.2% saponin in PBS for 16-24h at 4°C, blocked with 10% mouse serum in PBS for 16-24h, and stained with combinations of the following monoclonal antibodies diluted into a solution of 0.5% BSA, 5% mouse serum, and 0.1% saponin in PBS: Cy3-conjugated anti- α -smooth muscle actin (α SMA, 1:300, Sigma), AF594-conjugated anti-CD31 (1:100, BioLegend), AF647-conjugated anti-CD68 (1:200, AbD Serotec), and AF488-conjugated anti-CD206 (1:200, AbD Serotec). Images of dorsal tissue vessel networks were acquired as 3-dimensional z-stacked tile scans in confocal and multiphoton modes using a Zeiss LSM710 NLO microscope, Ti:Sapphire pulsed IR laser, and 5 \times , 10 \times , or 20 \times magnification. Male heterozygous B6.129P-Cx3cr1^{tm1Litt}/J (CX3CR1-EGFP) mice were utilized to visualize monocytes in live mice based on their selective surface expression of CX3CR1 [7, 17]. Intravital confocal visualization of CX₃CR1^{high} and CX₃CR1⁺ cells in/near peri-implant venules was performed in (CX3CR1-GFP) knock-in transgenic mice after jugular vein injection of rhodamine-conjugated isolectin B₄ (0.1mg/50 μ L; Vector Laboratories) to visualize perfused vasculature on day 1 after surgery. One 20 \times region of interest adjacent to each gel implant was imaged on day 1 after surgery and immediately after infusion of fluorescently tagged lectin to visualize vessels. Intravital confocal imaging was conducted with a 20 \times water immersion objective (NA=1.0). CX₃CR1⁺ cell numbers were quantified using Fiji and 3D surface rendering was performed in Imaris (Bitplane).

Statistical analysis

Data are presented as mean \pm standard error of the mean (SEM) unless otherwise indicated. Paired data for internally controlled studies were analyzed in paired *t*-tests or by ANOVA with repeated measures. Multiple comparisons were made by one- or two-way ANOVA followed by Bonferroni or Sidak post-tests to compare means. Linear regression analysis was performed separately on the internal control group and experimental group and r^2 values are reported. All statistical analysis was done in GraphPad Prism software. Unless otherwise noted, $p < 0.05$ was considered statistically significant.

Results

3.1: aHep^N hydrogels sustain release of bioactive of SDF-1 α *in vitro*

A selectively desulfated heparin PEG-DA hydrogel (Hep^N) was engineered to utilize the natural capacity of heparin to protect, sequester, and release growth factors as a novel

strategy to produce a localized *in vivo* gradient of SDF-1 α [27-29, 31, 35]. Fabrication and composition of heparin-containing hydrogels is illustrated in Figure 1A. SDF-1 α release from Hep^N gels incorporating albumin was superior to release from either unmodified PEG-DA, Hep^N-PEG-DA, or albumin-PEG-DA gels (Figure S2); therefore, in subsequent experiments, albumin was included in the Hep^N-PEG-DA hydrogels (aHep^N) to improve release of SDF-1 α . The albumin may help stabilize the protein from denaturation within the gel and since albumin is also negatively charged at neutral pH, may reduce growth factor binding to the gel and thus promote release [37, 38]. The albumin-containing, N-desulfated heparin-based hydrogels (aHep^N) chosen for this study released $9.8 \pm 0.1\%$ of the loaded SDF-1 α by 5h, $19.2 \pm 0.1\%$ by 24h, $23.1 \pm 0.1\%$ by day 3, and $23.8 \pm 0.0\%$ by day 7 *in vitro* (Figure 1B). Chemotaxis of primary murine bone marrow cells toward hydrogel conditioned media was analyzed to test the bioactivity of SDF-1 α released from the hydrogels. Media conditioned for 24h with aHep^N-SDF gels induced a statistically significant increase in directional chemotaxis ($27.22 \pm 9.5\%$) compared to release media from the same gels with no SDF-1 α (aHep^N), indicating that SDF-1 α bioactivity is retained after release from aHep^N hydrogels (Figure 1C).

3.2: aHep^N-SDF hydrogels locally recruit marrow-derived cells *in vivo*

The murine dorsal skinfold window chamber (“backpack”) model enables longitudinal spatiotemporal intravital imaging of host responses to biomaterial implants including remodeling of vessel networks and coupled innate immune response [17, 19]. To evaluate the *in vivo* recruitment of circulating cells to the gels, we generated mouse chimeras whose bone marrow-derived hematopoietic lineage cells express a constitutive enhanced green fluorescent protein (EGFP) transgene. Chimeric mice fitted with dorsal skinfold windows permit the tracking of cells originating from the bone marrow and arriving at the injury niche. The experimental design was internally controlled to evaluate a localized biological response around the gel by implanting one aHep^N-SDF (“experimental”) gel and one Hep^N (“internal control”) hydrogel into opposite sides of the same window (less than 8mm separation between center of each gel) (Figure 2A, B). Whole mount immunofluorescence microscopy analysis of dorsal skinfold tissue 2 days after surgical tissue disruption and hydrogel implantation showed that the aHep^N-SDF hydrogel appeared to recruit more bone marrow-derived (EGFP⁺) circulating cells than internal control hydrogels in the same dorsal skinfold window chamber (Figure 2C). Moreover, the spatial distribution of recruited bone marrow-derived cells was localized to the SDF-1 α implant niche, as indicated by higher trend in EGFP fluorescence underneath the SDF-1 α -releasing gels compared to paired internal controls in all 3 animals ($p=0.1$; Figure 2C, D).

3.3: aHep^N-SDF hydrogels enhance local recruitment of anti-inflammatory monocytes

To further evaluate the identity and localization of recruited cells, wildtype C57/BL6 mice were implanted with one experimental (aHep^N or aHep^N-SDF) gel and one internal control unloaded gel (Hep^N) as described above (Figure 3A). Brightfield microscopy of explanted hydrogels revealed loose cell attachment to the tissue-implant interface at day 3 with no apparent differences between groups (Figure 3B). Cells were digested from the surface of the gels and analyzed by flow cytometry. SDF-1 α delivery did not significantly affect the number of myeloid leukocytes (CD11b⁺) or cells expressing the SDF-1 α receptor

(CXCR4⁺) attached to the hydrogel (Figure 3B-D). To examine the phenotypes of recruited cells in the tissue surrounding each implant, dorsal tissue was harvested and bisected along the midline separating the two hydrogels (Figure 4A). The proportion of CD11b⁺ cells out of total cells in the digested dorsal tissue was not different between groups (Figure 4B); however, hydrogels releasing SDF-1 α significantly increased the tissue recruitment of AMs (CD11b⁺SSC^{lo}Ly-6C^{lo}) compared to aHep^{-N} animals (Figure 4C). Local infiltration of IMs (CD11b⁺SSC^{low}Ly-6C^{high}) was not significantly different between unloaded and SDF-1 α -loaded aHep^{-N} gels (Figure 4D). The ratio of AM to IM was significantly higher in the tissue surrounding the SDF-1 α releasing hydrogels compared to both the Hep^{-N} internal control and the aHep^{-N} experimental control hydrogels (Figure 4E). To gain mechanistic insight into the preferential recruitment of AMs by SDF-1 α , we analyzed the cell surface expression of the SDF-1 α cognate receptor, CXCR4. Bone marrow-derived AMs have higher surface expression of CXCR4 compared to IMs (Figure 4F) These data suggest that the SDF-1 α releasing hydrogel preferentially attracts the pro-regenerative AM subset of monocytes to the tissue surrounding the gel, which is in accordance with our previous work showing that AMs migrate toward SDF-1 α significantly more than IMs [16].

3.4: Early arteriolar vascular expansion is correlated with AM recruitment

Previous reports suggest that perivascular positioning of monocytes and macrophages promotes vascular remodeling [17, 21, 42]; therefore we utilized intravital confocal laser microscopy analysis of post-capillary venules to examine the infiltration and positioning of CX3CR1-EGFP⁺ monocytes (Figure 5A, B, green) with respect to vessels (Figure 5A, B, red) in the peri-implant region. Images were further processed with Imaris software to generate 3D surface renderings and visualize cell proximity to vessels; a 3D distance heat map was overlaid on the cells (Figure 5C, D). Significantly more CX3CR1⁺ cells were observed in regions of interest around the aHep^{-N}-SDF hydrogels on day 1 after dorsal window chamber placement (Figure 5E; 68 ± 17 cells (Hep^{-N}) vs. 127 ± 88 (aHep^{-N}-SDF) in 0.49mm^2 area; n=3 mice). Early recruitment of CX3CR1^{high} AM cells was also observed (10 ± 4 cells (Hep^{-N}) vs. 22 ± 10 (aHep^{-N}-SDF); n=3 mice) in agreement with our finding that SDF-1 α delivery increases recruitment of AMs.

Longitudinal intravital brightfield microscopy analysis of hydrogel-treated dorsal tissue at days 0 and 3 does not show significant changes between groups in the diameter of peri-implant arterioles with an initial diameter less than $40\mu\text{m}$ (Figure 5F); however the change in arteriolar diameter in aHep^{-N}-SDF animals relative to the internal control was significantly higher than aHep^{-N} relative to its internal control (Figure 5G, n=3-4 mice per group, # $p < 0.05$, one-way t-test). Linear regression analysis of paired immunophenotyping (by flow cytometry) and vessel measurements (by intravital imaging) indicates that arteriolar diameter enlargement positively correlates with AM:IM ratio in peri-implant tissue for both the SDF-1 α - loaded and unloaded controls (Figure 5H). SDF-1 α increased the slope of the regression line compared to unloaded gels suggesting that SDF-1 α may amplify the positive effects of AM recruitment with respect to arteriolar diameter increase (Figure 5H).

3.5: Hydrogel release of SDF-1 α sustains local arteriolar expansion and microvascular network growth

SDF-1 α release maintained peri-implant arteriolar structural enlargement at day 7 (Figure 6A-C, S3). All animals exhibited a positive arteriolar enlargement response to SDF-1 α release from aHep^N-SDF gels compared to internal control while aHep^N gels did not differ from internal controls (Figure 6B). Accordingly, the change in arteriolar diameter in aHep^N-SDF relative to the internal control was significantly higher than aHep^N relative to its internal control (Figure 6C; $-2.45\% \pm 10.55\%$ (aHep^N) vs. $24.10\% \pm 6.43\%$ (aHep^N-SDF); $n=3-5$). We hypothesized that the sustained pro-arteriogenic response may be supported by the persistence of recruited AMs through their differentiation into macrophages, particularly of the M2 phenotype associated with regeneration [17, 43]. CD206⁺ M2-like macrophages were identified in a peri-arteriolar niche location (Figure 6D), a phenomenon previously associated with arteriogenesis [41].

In addition to rapid changes in perfusion that can be accommodated by arteriogenic changes in local vasculature, angiogenic microvascular network growth is another hallmark of regenerative vascular remodeling. Analysis of network length in brightfield intravital microscopy was unable to detect differences in vessel length density between groups (Figure 6E, 7A-B) perhaps due to the resolution limit of this technique (approximately 20-25 μ m). However, whole mount CD31 immunostaining of perfusion-fixed, explanted dorsal skin enabled visualization of capillary-level microcirculation undetectable by brightfield imaging (Figure 7C-F, S4). Tissue surrounding internal control hydrogels appeared to be more optically opaque in brightfield imaging (Figure S3), possibly indicating the formation of granulation tissue that may obscure visualization of microvessels. SDF-1 α delivery from aHep^N-SDF hydrogels significantly increased the density of CD31⁺ vessels near the implant compared to internal control less than 8mm away in the window chamber at day 7 (Figure 7E-G). These data support the idea of highly localized regenerative capacity of bioactive SDF-1 α released from a heparin-based hydrogel *in vivo*.

Discussion

Stimulating the expansion of stable vascular networks promises to improve therapeutic outcomes after ischemia, trauma, and tissue transplantation; however, engineering a therapy that potently and safely promotes vascularization remains an unmet clinical need. Spatial concentration of pro-angiogenic/arteriogenic therapies would minimize off-target risks such as stimulating rogue tumor vasculature [44, 45], while focusing treatment only to the injured or regenerating tissue region. Here we exploited the ability of PEG-DA hydrogels functionalized with N-desulfated heparin, a modified GAG, to localize the presentation of bioactive growth factor cargo SDF-1 α [28] and spatially concentrate its pro-angiogenic/arteriogenic effects. Selectively desulfated heparin exhibits low anticoagulant activity compared to native heparin while still protecting bioactivity of growth factor cargo [28, 29, 31, 35].

SDF-1 α is of interest in angiogenic/arteriogenic therapies because pathophysiologically, SDF-1 α can be secreted perivascularly by vessel-associated cells downstream of VEGF signaling, contributing to positioning of monocytes within a localized gradient of SDF-1 α at

the outer vessel wall [21]. While recruitment of monocytes has been associated with pro-angiogenic and arteriogenic metrics [17, 21, 25, 42, 46-48], the phenotype of SDF-1 α -recruited cells has not been well characterized. Literature strongly associates both arteriogenesis and angiogenesis with recruitment of Ly-6C^{lo} AMs and M2-like macrophages [17, 19, 49, 50]. We found that AMs have higher surface expression of CXCR4 (Figure 4F), therefore yielding them more sensitive to SDF-1 α chemotactic signals compared to IMs. These data are in agreement with our recent finding that SDF-1 α -directed chemotaxis is higher for AMs than IMs [17]. Indeed, in the present study we showed that heparin-functionalized hydrogels exhibiting *in vitro* release of SDF-1 α over 3 days achieved increased monocyte recruitment to the peri-hydrogel space *in vivo* as early as 1 day compared to internal control (Figure 5E). Three days after surgery, more AMs were recruited to the aHep^N-SDF gel than the aHep^N gel without SDF-1 (Figure 4C). Similarly, the ratio of AM to IM cells was significantly higher under the aHep^N-SDF gel compared to the Hep^N gel less than 8mm away indicating a shift in the local tissue environment from inflammatory to regenerative (Figure 4E). These data suggest that the aHep^N-SDF hydrogel achieves a high degree of spatial control in pro-regenerative endogenous cell recruitment that enables continued cellular therapeutic action outlasting SDF-1 α release.

Monocytes and monocyte-derived macrophages are key players in promoting angiogenesis and arteriogenesis, making them a desirable endogenous cell source to target for pro-regenerative immunologically smart biomaterials. During inflammatory vascular remodeling, select populations of perivascular monocytes and macrophages contribute paracrine signals to the remodeling vasculature, including secretion of growth factors such as platelet-derived growth factor (PDGF) and VEGF, as well as matrix-remodeling enzymes such as MMPs [21, 25, 42, 47, 48]. Consistent with this supportive role of monocytes and macrophages in vascular remodeling, we showed in the present study that SDF-1 α -releasing aHep^N hydrogels promoted the influx and retention of pro-regenerative monocytes that correlated with enhanced early and sustained arteriogenesis of small arterioles (< 40 μ m) and enhanced microvascular network density in the tissue surrounding SDF-1 α releasing aHep^N-SDF hydrogels (Figure 4-7). Thus, localized SDF-1 α delivery may increase blood flow critical for tissue repair processes, in part through early and selective recruitment of pro-regenerative monocytes. Intravital imaging allowed us to use paired data of change in vessel diameter and immunophenotype of monocytes around the gels. Early arteriolar structural changes correlated with the AM:IM ratio in tissue and the slope of the aHep^N-SDF regression line was higher than internal control. The difference in slope between the internal control and aHep^N-SDF gels could suggest that local SDF-1 α further enhances the pro-arteriogenic activity of recruited AMs locally through additional functional cues. Indeed, previous reports have suggested that VEGF induces “on-site education” of monocytes upon recruitment, functioning both as a recruitment signal and a knob to tune pro-regenerative function of the arriving cells [25]. Taken together, our data suggest that the aHep^N-SDF hydrogel system is a promising “immune-regenerative engineering” approach to promote vascularization in injured tissue through recruitment of anti-inflammatory monocytes to the injury niche to enable or enhance their therapeutic potential.

Supplementary Material

Refer to Web version on PubMed Central for supplementary material.

Acknowledgments

We thank the core facilities staff of the Parker H. Petit Institute for Bioengineering and Bioscience for technical expertise and assistance. In addition we thank the Emory University Integrated Cellular Imaging Microscopy Core for their expertise and assistance in image analysis. Sources of support for this study include the National Institutes of Health grants K01AR052352-01A1, R01AR056445-01A2, and R01DE019935-01 to Dr. Botchwey and Petit Faculty Fellowship funds for Dr. Temenoff.

References

1. Ginhoux F, Jung S. Monocytes and macrophages: developmental pathways and tissue homeostasis. *Nature reviews Immunology*. 2014; 14:392–404.
2. Hur J, Choi JI, Yun JY, Yoon CH, Jang JH, Im SG, et al. Highly angiogenic CXCR4(+)CD31(+) monocyte subset derived from 3D culture of human peripheral blood. *Biomaterials*. 2013; 34:1929–41. [PubMed: 23267826]
3. Patel AS, Smith A, Nucera S, Biziato D, Saha P, Attia RQ, et al. TIE2-expressing monocytes/macrophages regulate revascularization of the ischemic limb. *EMBO molecular medicine*. 2013; 5:858–69. [PubMed: 23653322]
4. Shantsila E, Tapp LD, Wrigley BJ, Montoro-Garcia S, Lip GY. CXCR4 positive and angiogenic monocytes in myocardial infarction. *Thrombosis and haemostasis*. 2013; 109:255–62. [PubMed: 23223950]
5. Zhang Z, Shively JE. Acceleration of bone repair in NOD/SCID mice by human monoosteophils, novel LL-37-activated monocytes. *PloS one*. 2013; 8:e67649. [PubMed: 23844045]
6. Swirski FK, Nahrendorf M, Etzrodt M, Wildgruber M, Cortez-Retamozo V, Panizzi P, et al. Identification of splenic reservoir monocytes and their deployment to inflammatory sites. *Science*. 2009; 325:612–6. [PubMed: 19644120]
7. Geissmann F, Jung S, Littman DR. Blood monocytes consist of two principal subsets with distinct migratory properties. *Immunity*. 2003; 19:71–82. [PubMed: 12871640]
8. Yona S, Kim KW, Wolf Y, Mildner A, Varol D, Breker M, et al. Fate mapping reveals origins and dynamics of monocytes and tissue macrophages under homeostasis. *Immunity*. 2013; 38:79–91. [PubMed: 23273845]
9. Aurora AB, Porrello ER, Tan W, Mahmoud AI, Hill JA, Bassel-Duby R, et al. Macrophages are required for neonatal heart regeneration. *The Journal of clinical investigation*. 2014; 124:1382–92. [PubMed: 24569380]
10. Leuschner F, Rauch PJ, Ueno T, Gorbатов R, Marinelli B, Lee WW, et al. Rapid monocyte kinetics in acute myocardial infarction are sustained by extramedullary monocytopoiesis. *The Journal of experimental medicine*. 2012; 209:123–37. [PubMed: 22213805]
11. Nahrendorf M, Swirski FK, Aikawa E, Stangenberg L, Wurdinger T, Figueiredo JL, et al. The healing myocardium sequentially mobilizes two monocyte subsets with divergent and complementary functions. *The Journal of experimental medicine*. 2007; 204:3037–47. [PubMed: 18025128]
12. Zhang Z, Shively JE. Generation of novel bone forming cells (monoosteophils) from the cathelicidin-derived peptide LL-37 treated monocytes. *PloS one*. 2010; 5:e13985. [PubMed: 21085494]
13. Shechter R, Miller O, Yovel G, Rosenzweig N, London A, Ruckh J, et al. Recruitment of beneficial M2 macrophages to injured spinal cord is orchestrated by remote brain choroid plexus. *Immunity*. 2013; 38:555–69. [PubMed: 23477737]
14. Shechter R, Schwartz M. Harnessing monocyte-derived macrophages to control central nervous system pathologies: no longer ‘if’ but ‘how’. *The Journal of pathology*. 2013; 229:332–46. [PubMed: 23007711]

15. Godwin JW, Pinto AR, Rosenthal NA. Macrophages are required for adult salamander limb regeneration. *Proceedings of the National Academy of Sciences of the United States of America*. 2013; 110:9415–20. [PubMed: 23690624]
16. Mosser DM, Edwards JP. Exploring the full spectrum of macrophage activation. *Nature reviews Immunology*. 2008; 8:958–69.
17. Awojoodu AO, Ogle ME, Sefcik LS, Bowers DT, Martin K, Brayman KL, et al. Sphingosine 1-phosphate receptor 3 regulates recruitment of anti-inflammatory monocytes to microvessels during implant arteriogenesis. *Proceedings of the National Academy of Sciences of the United States of America*. 2013; 110:13785–90. [PubMed: 23918395]
18. Christoffersson G, Vagesjo E, Vandooren J, Liden M, Massena S, Reinert RB, et al. VEGF-A recruits a proangiogenic MMP-9-delivering neutrophil subset that induces angiogenesis in transplanted hypoxic tissue. *Blood*. 2012; 120:4653–62. [PubMed: 22966168]
19. Ogle ME, Sefcik LS, Awojoodu AO, Chiappa NF, Lynch K, Peirce-Cottler S, et al. Engineering in vivo gradients of sphingosine-1-phosphate receptor ligands for localized microvascular remodeling and inflammatory cell positioning. *Acta biomaterialia*. 2014; 10:4704–14. [PubMed: 25128750]
20. Stark K, Eckart A, Haidari S, Tirniceriu A, Lorenz M, von Bruhl ML, et al. Capillary and arteriolar pericytes attract innate leukocytes exiting through venules and ‘instruct’ them with pattern-recognition and motility programs. *Nature immunology*. 2013; 14:41–51. [PubMed: 23179077]
21. Grunewald M, Avraham I, Dor Y, Bachar-Lustig E, Itin A, Jung S, et al. VEGF-induced adult neovascularization: recruitment, retention, and role of accessory cells. *Cell*. 2006; 124:175–89. [PubMed: 16413490]
22. Omatsu Y, Seike M, Sugiyama T, Kume T, Nagasawa T. Foxc1 is a critical regulator of haematopoietic stem/progenitor cell niche formation. *Nature*. 2014; 508:536–40. [PubMed: 24590069]
23. Otsuru S, Tamai K, Yamazaki T, Yoshikawa H, Kaneda Y. Circulating bone marrow-derived osteoblast progenitor cells are recruited to the bone-forming site by the CXCR4/stromal cell-derived factor-1 pathway. *Stem cells*. 2008; 26:223–34. [PubMed: 17932420]
24. Zemani F, Silvestre JS, Fauvel-Lafeve F, Bruel A, Vilar J, Bieche I, et al. Ex vivo priming of endothelial progenitor cells with SDF-1 before transplantation could increase their proangiogenic potential. *Arteriosclerosis, thrombosis, and vascular biology*. 2008; 28:644–50.
25. Avraham-Davidi I, Yona S, Grunewald M, Landsman L, Cochain C, Silvestre JS, et al. On-site education of VEGF-recruited monocytes improves their performance as angiogenic and arteriogenic accessory cells. *The Journal of experimental medicine*. 2013; 210:2611–25. [PubMed: 24166715]
26. Ehling J, Bartneck M, Wei X, Gremse F, Fech V, Mockel D, et al. CCL2-dependent infiltrating macrophages promote angiogenesis in progressive liver fibrosis. *Gut*. 2014; 63:1960–71. [PubMed: 24561613]
27. Hettiaratchi MH, Miller T, Temenoff JS, Guldborg RE, McDevitt TC. Heparin microparticle effects on presentation and bioactivity of bone morphogenetic protein-2. *Biomaterials*. 2014; 35:7228–38. [PubMed: 24881028]
28. Seto SP, Miller T, Temenoff JS. Effect of selective heparin desulfation on preservation of bone morphogenetic protein-2 bioactivity after thermal stress. *Bioconjugate chemistry*. 2015; 26:286–93. [PubMed: 25621929]
29. Tellier LE, Miller T, McDevitt TC, Temenoff JS. Hydrolysis and sulfation pattern effects on release of bioactive bone morphogenetic protein-2 from heparin-based microparticles. *Journal of Materials Chemistry B*. 2015; 3:8001–9.
30. Sadir R, Baleux F, Grosdidier A, Imberty A, Lortat-Jacob H. Characterization of the stromal cell-derived factor-1 α -heparin complex. *The Journal of biological chemistry*. 2001; 276:8288–96. [PubMed: 11087743]
31. Miller T, Goude MC, McDevitt TC, Temenoff JS. Molecular engineering of glycosaminoglycan chemistry for biomolecule delivery. *Acta biomaterialia*. 2014; 10:1705–19. [PubMed: 24121191]
32. Inoue Y, Nagasawa K. Selective N-desulfation of heparin with dimethyl sulfoxide containing water or methanol. *Carbohydr Res*. 1976; 46:87–95. [PubMed: 1248016]

33. Hricovini M, Guerrini M, Bisio A, Torri G, Naggi A, Casu B. Active conformations of glycosaminoglycans. NMR determination of the conformation of heparin sequences complexed with antithrombin and fibroblast growth factors in solution. *Semin Thromb Hemost.* 2002; 28:325–34. [PubMed: 12244479]
34. Levy L, Petracek FJ. Chemical and pharmacological studies on N-resulfated heparin. *Proc Soc Exp Biol Med.* 1962; 109:901–5. [PubMed: 14464789]
35. Nakamura S, Ishihara M, Obara K, Masuoka K, Ishizuka T, Kanatani Y, et al. Controlled release of fibroblast growth factor-2 from an injectable 6-O-desulfated heparin hydrogel and subsequent effect on in vivo vascularization. *J Biomed Mater Res A.* 2006; 78:364–71. [PubMed: 16673389]
36. Roy S, Lai H, Zouaoui R, Duffner J, Zhou H, L PJ, et al. Bioactivity screening of partially desulfated low-molecular-weight heparins: a structure/activity relationship study. *Glycobiology.* 2011; 21:1194–205. [PubMed: 21515908]
37. Hawe A, Friess W. Stabilization of a hydrophobic recombinant cytokine by human serum albumin. *Journal of pharmaceutical sciences.* 2007; 96:2987–99. [PubMed: 17786949]
38. Zamani M, Prabhakaran MP, Thian ES, Ramakrishna S. Controlled delivery of stromal derived factor-1alpha from poly lactic-co-glycolic acid core-shell particles to recruit mesenchymal stem cells for cardiac regeneration. *J Colloid Interface Sci.* 2015; 451:144–52. [PubMed: 25897850]
39. Sefcik LS, Aronin CE, Awojoodu AO, Shin SJ, Mac Gabhann F, MacDonald TL, et al. Selective activation of sphingosine 1-phosphate receptors 1 and 3 promotes local microvascular network growth. *Tissue engineering Part A.* 2011; 17:617–29. [PubMed: 20874260]
40. Sefcik LS, Petrie Aronin CE, Wiegand KA, Botchwey EA. Sustained release of sphingosine 1-phosphate for therapeutic arteriogenesis and bone tissue engineering. *Biomaterials.* 2008; 29:2869–77. [PubMed: 18405965]
41. Bruce AC, Kelly-Goss MR, Heuslein JL, Meisner JK, Price RJ, Peirce SM. Monocytes are recruited from venules during arteriogenesis in the murine spinotrapezius ligation model. *Arteriosclerosis, thrombosis, and vascular biology.* 2014; 34:2012–22.
42. Fantin A, Vieira JM, Gestri G, Denti L, Schwarz Q, Prykhodzhiy S, et al. Tissue macrophages act as cellular chaperones for vascular anastomosis downstream of VEGF-mediated endothelial tip cell induction. *Blood.* 2010; 116:829–40. [PubMed: 20404134]
43. Kigerl KA, Gensel JC, Ankeny DP, Alexander JK, Donnelly DJ, Popovich PG. Identification of two distinct macrophage subsets with divergent effects causing either neurotoxicity or regeneration in the injured mouse spinal cord. *The Journal of neuroscience : the official journal of the Society for Neuroscience.* 2009; 29:13435–44. [PubMed: 19864556]
44. Ratajczak MZ, Kim CH, Abdel-Latif A, Schneider G, Kucia M, Morris AJ, et al. A novel perspective on stem cell homing and mobilization: review on bioactive lipids as potent chemoattractants and cationic peptides as underappreciated modulators of responsiveness to SDF-1 gradients. *Leukemia.* 2012; 26:63–72. [PubMed: 21886175]
45. Ratajczak MZ, Zuba-Surma E, Kucia M, Reza R, Wojakowski W, Ratajczak J. The pleiotropic effects of the SDF-1-CXCR4 axis in organogenesis, regeneration and tumorigenesis. *Leukemia.* 2006; 20:1915–24. [PubMed: 16900209]
46. Arras M, Ito WD, Scholz D, Winkler B, Schaper J, Schaper W. Monocyte activation in angiogenesis and collateral growth in the rabbit hindlimb. *The Journal of clinical investigation.* 1998; 101:40–50. [PubMed: 9421464]
47. Ito WD, Arras M, Winkler B, Scholz D, Schaper J, Schaper W. Monocyte chemotactic protein-1 increases collateral and peripheral conductance after femoral artery occlusion. *Circulation research.* 1997; 80:829–37. [PubMed: 9168785]
48. Troidl C, Jung G, Troidl K, Hoffmann J, Mollmann H, Nef H, et al. The temporal and spatial distribution of macrophage subpopulations during arteriogenesis. *Current vascular pharmacology.* 2013; 11:5–12. [PubMed: 23391417]
49. Mantovani A, Sozzani S, Locati M, Allavena P, Sica A. Macrophage polarization: tumor-associated macrophages as a paradigm for polarized M2 mononuclear phagocytes. *Trends in immunology.* 2002; 23:549–55. [PubMed: 12401408]

50. Takeda Y, Costa S, Delamarre E, Roncal C, Leite de Oliveira R, Squadrito ML, et al. Macrophage skewing by Phd2 haplodeficiency prevents ischaemia by inducing arteriogenesis. *Nature*. 2011; 479:122–6. [PubMed: 21983962]

Author Manuscript

Author Manuscript

Author Manuscript

Author Manuscript

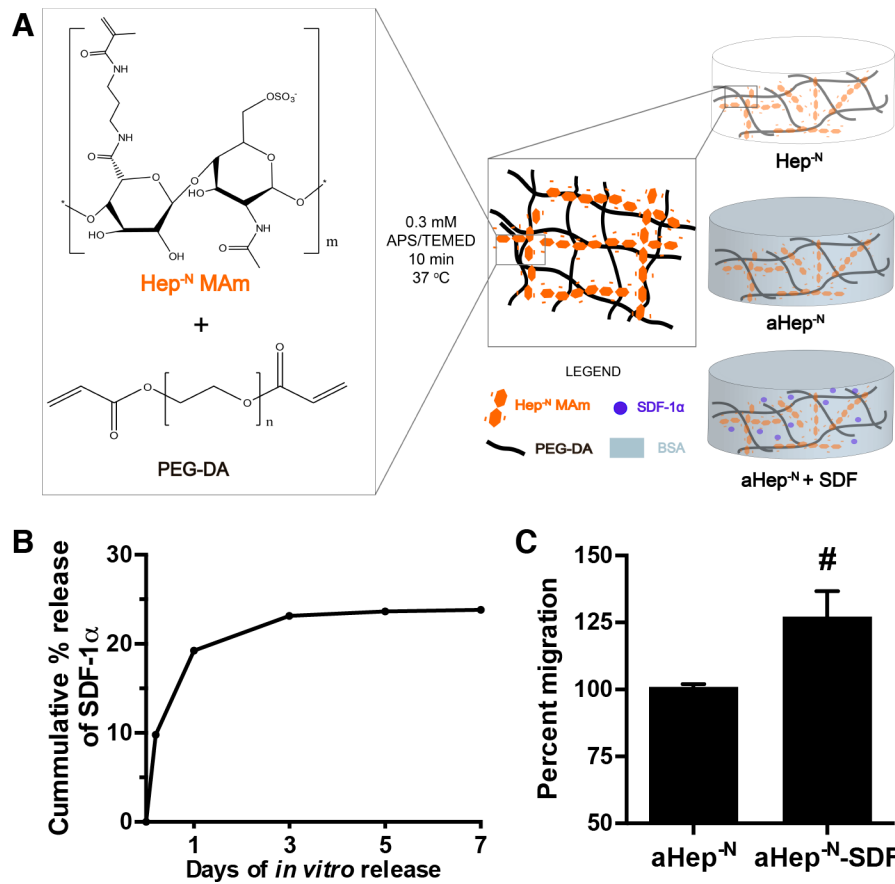


Figure 1. aHep^N hydrogel provides sustained release of bioactive SDF-1α

(A) Hydrogels were fabricated by thermal cross-linking of N-desulfated heparin methacrylamide and PEG-DA. Hydrogel formulations used in this study were: unloaded (Hep^N) internal controls, albumin loaded (aHep^N), or SDF-1α and albumin loaded (aHep^N-SDF). (B) SDF-1α release from aHep^N-SDF hydrogels is sustained over 3 days *in vitro* (n=3, mean ± SD) and (C) stimulates chemotaxis of mouse bone marrow cells *in vitro* (#p<0.05, unpaired t-test, n=4, mean ± SEM).

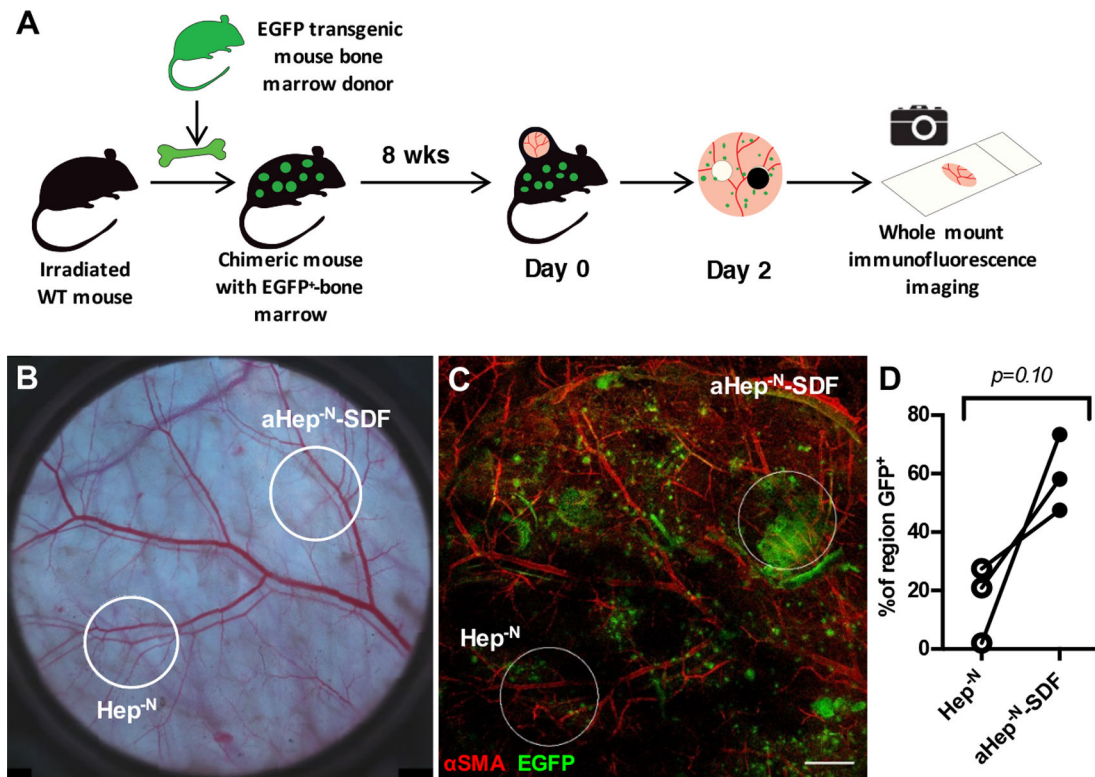


Figure 2. SDF-1 α recruits bone marrow-derived cells to the hydrogel implant niche
 (A) Chimeric mice were generated as illustrated by irradiation and bone marrow transplantation from an EGFP transgenic mouse. (B) Brightfield tiled image of dorsal skinfold window chamber on day 0 with location of aHep^N-SDF and internal control gels. (C) Rendering of Z-stacked tile scans acquired via confocal laser scanning microscopy show that more EGFP⁺ bone marrow-derived cells (green) are recruited to the tissue beneath aHep^N-SDF hydrogels compared to Hep^N internal control and recruitment is highly localized. Vessels are counterstained with α SMA (red). (D) Percent area under the gel positive for GFP. Lines connect paired analysis of internal control and experimental gels in each animal ($p=0.1$ by paired t-test, $n=3$; scale bar = 1mm).

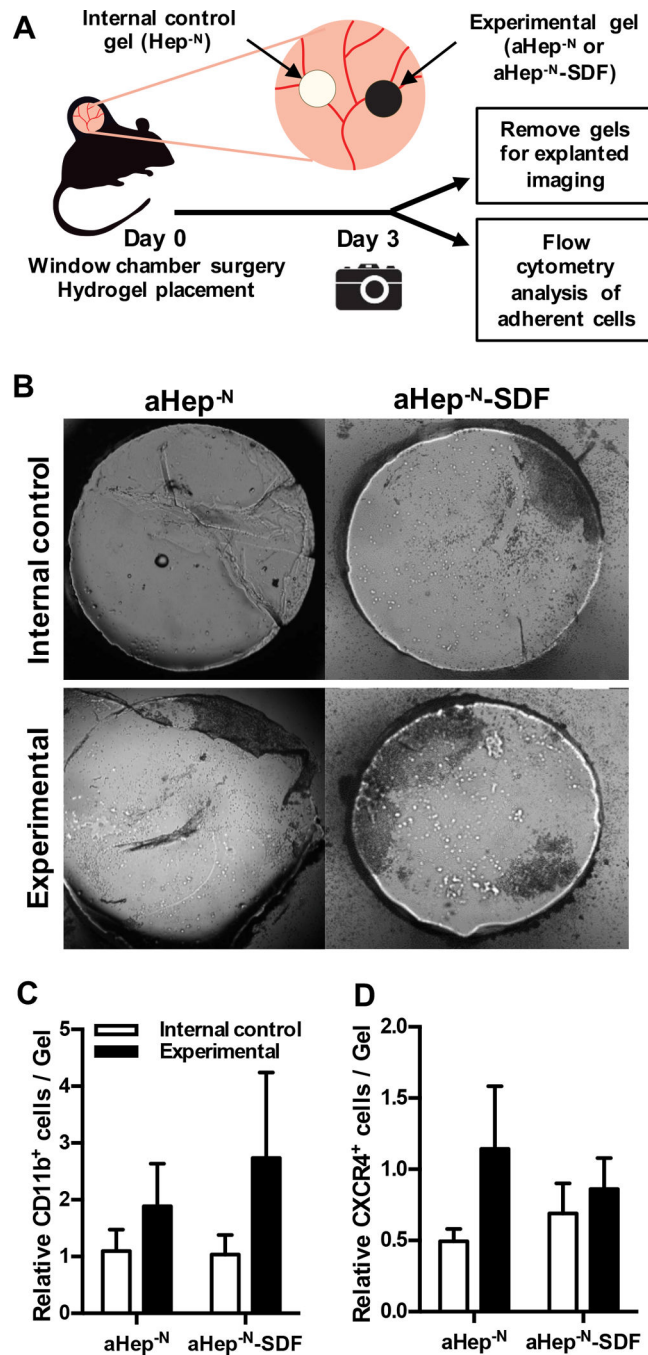


Figure 3. *In vivo* recruitment of cells to the hydrogel interface

(A) Hydrogels were explanted on day 3 for imaging and flow cytometry analysis of attached cells. (B) Some cells were attached to explanted hydrogels on day 3 but no significant differences in attachment of (C) CD11b⁺ and (D) CXCR4⁺ cell populations were measured between groups by flow cytometry (n=4-6 mice from 2 independent experiments, mean ± SEM).

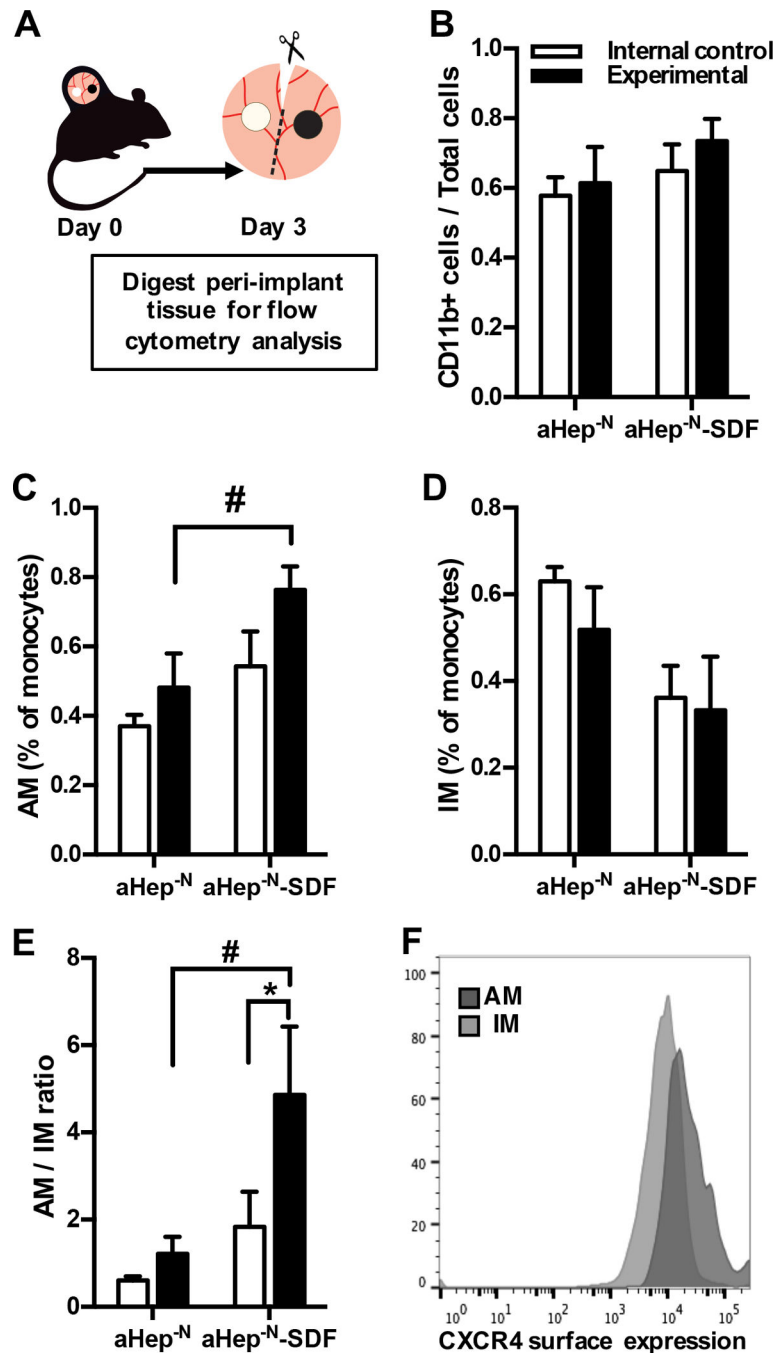


Figure 4. Localized recruitment of anti-inflammatory monocytes to the tissue surrounding the aHep^N-SDF hydrogel

(A) Tissue was bisected between the internal control (Hep^N, white) and the experimental (aHep^N or aHep^N-SDF, black) gels, digested with collagenase, and analyzed by flow cytometry. (B) The proportion of CD11b cells in the implant niche is not significantly different between groups. (C) aHep^N-SDF hydrogels induce a significant increase in the recruitment of AM, but not IM (D) to the peri-hydrogel tissue. (E) The ratio of AM to IM in the tissue surrounding aHep^N-SDF hydrogels is higher than aHep^N experimental control and Hep^N internal control. (F) Surface expression of the SDF-1 α cognate receptor CXCR4

is higher on the surface of AM compared to IM. (#, * $p < 0.05$: two-way ANOVA with repeated measures and Bonferonni test for multiple comparisons; $n=5$ mice from 2 independent experiments, mean \pm SEM).

Author Manuscript

Author Manuscript

Author Manuscript

Author Manuscript

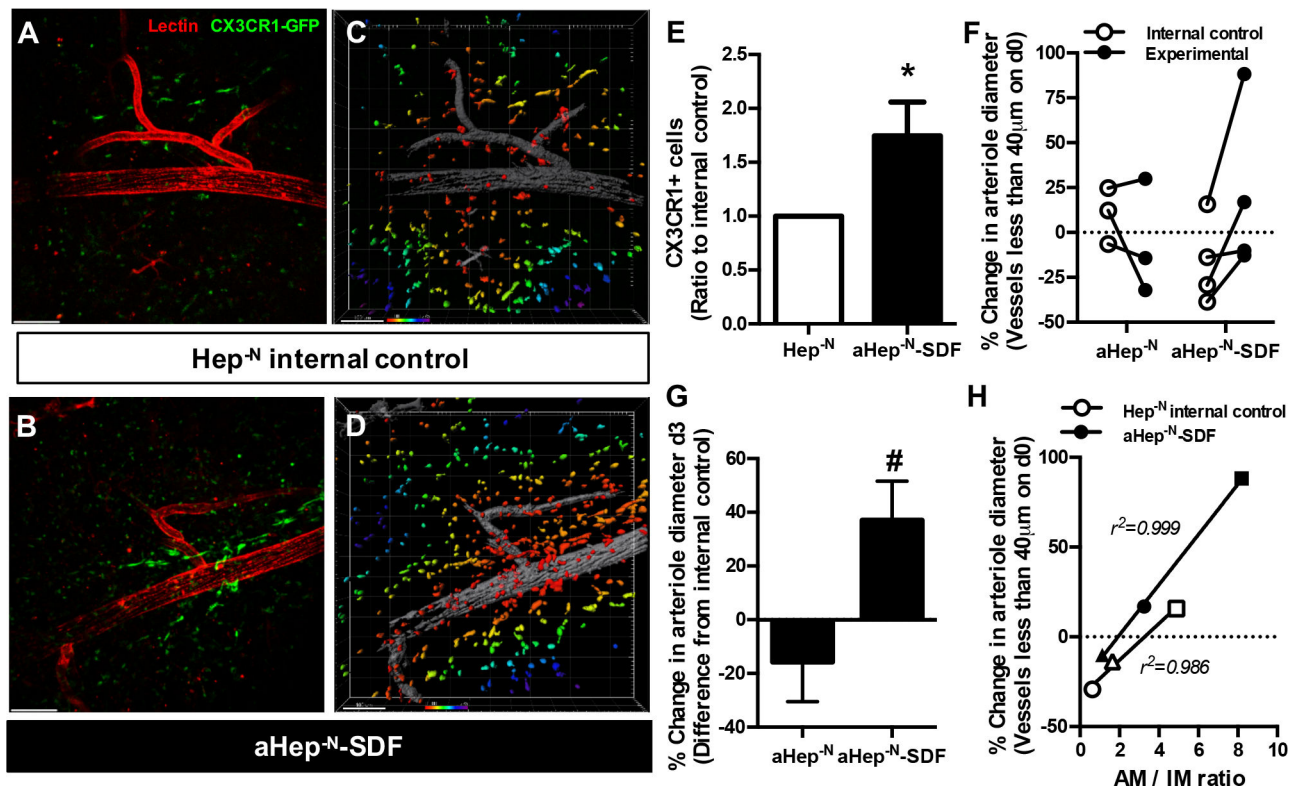


Figure 5. Monocyte recruitment correlates with early arteriolar remodeling

(A, B) Representative intravital imaging adjacent to each gel 1 day after surgery in CX3CR1-eGFP mice. (C, D) Color-coded map of 3D distance of CX3CR1+ cells from the surface of vessels rendered in Imaris software shows increased distribution of monocytes near vessels (perfused lectin, grey) near the aHep^N-SDF gel (scale bar = 100 μ m, color scale: 0.00 to 0.275mm distance to vessel). (E) SDF-1 α release increases perivascular CX3CR1+ cells ($*p < 0.05$, paired ratio t-test, $n = 3$, mean \pm SEM). (F) The percent change in arteriolar diameter from day 0 is not significantly changed on day 3 (Lines connect paired analysis of internal control and experimental gels in each animal); however, (G) the change from internal control significantly increased ($\#p < 0.05$, one-tailed t-test, $n = 3-4$, mean \pm SEM). (H) The change in vessel diameter is highly correlated to the balance of AM and IM recruited to the tissue (linear regression of paired data, $n = 3$, $m = 14.0 \pm 0.4$, $r^2 = 0.986$ for aHep^N-SDF; $m = 10.2 \pm 1.2$, $r^2 = 0.999$ for Hep^N).

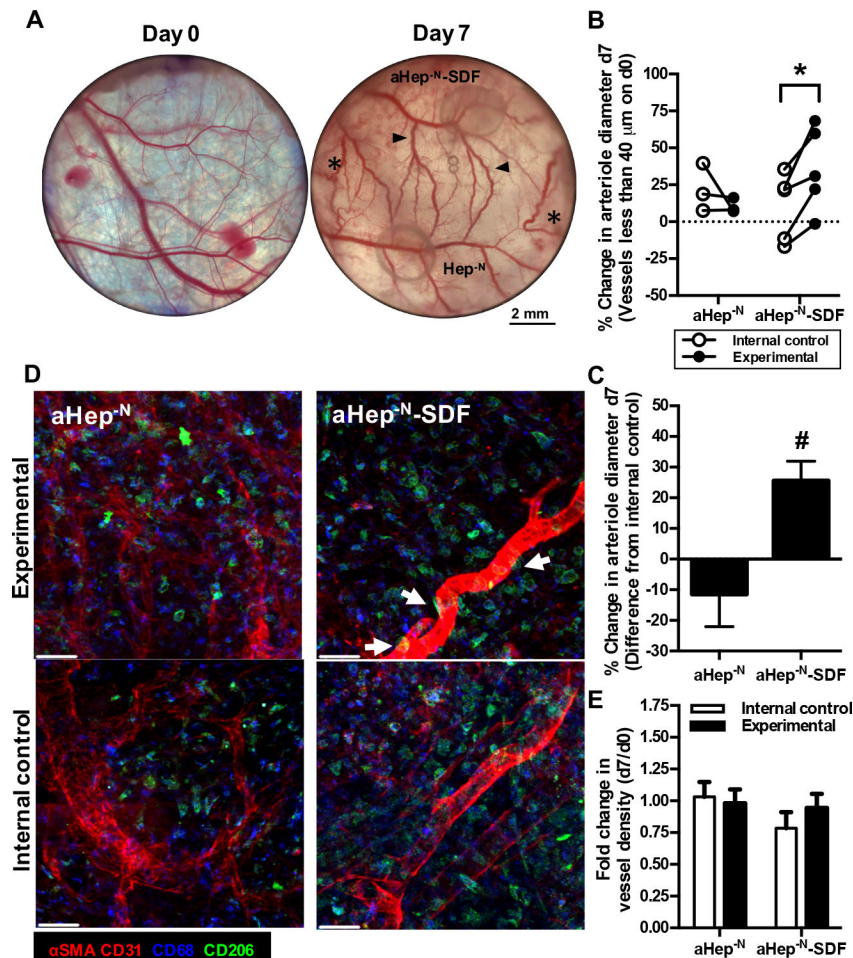


Figure 6. aHep^{-N}-SDF hydrogels sustain inflammatory arteriolar remodeling

(A) Dorsal skinfold tissue treated with aHep^{-N}-SDF hydrogels increases vessel caliber (arrowheads) and tortuosity (asterisks) by day 7 (Scale bar 2mm). (B) All animals display significantly increased arteriolar diameter near aHep^{-N}-SDF hydrogels compared to internal controls. (* $p < 0.05$ by two-way ANOVA with repeated measures and Bonferonni test for multiple comparisons, $n=3-5$ from 2 independent experiments, lines connect paired analysis of internal control and experimental gels in each animal). (C) The relative increase in arteriolar diameter above internal control is significantly higher in the aHep^{-N}-SDF group compared to aHep^{-N} control (# $p < 0.05$, t-test, $n=3-5$ mice, mean \pm SEM). (D) CD206⁺ M2-like macrophages were identified in the tissue beneath aHep^{-N}-SDF hydrogels and associated internal controls (red, CD31 and α SMA; blue, CD68; green, CD206; scale bar = 50 μ m). M2-like macrophages were localized in a peri-arteriolar niche (arrowheads). Lower panels: internal control Hep^{-N} gels. (E) Analysis of microvessel density in intravital brightfield images was unable to detect a difference in microvessel network length in the injury niche ($n=3-4$ mice per group, mean \pm SEM).

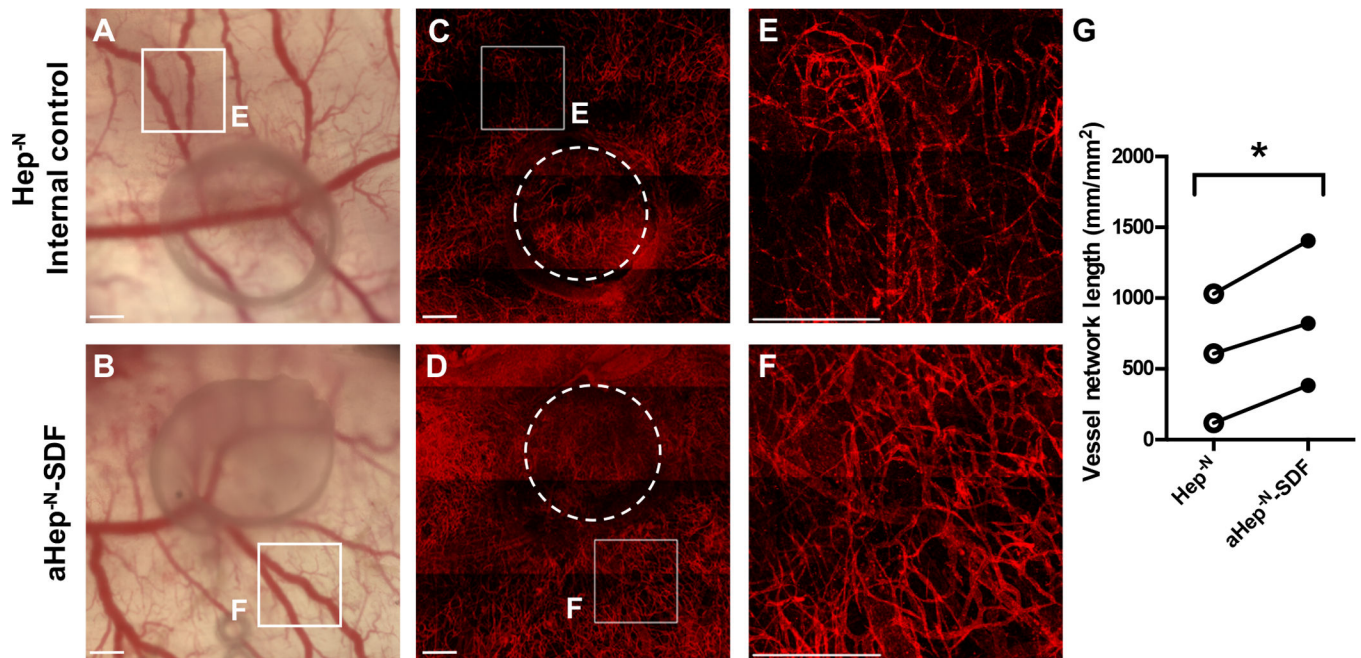


Figure 7. aHep^N-SDF hydrogels enhance inflammatory microvascular network growth
 (A, B) Intravital brightfield microscopy and (C, D) CD31⁺ whole mount immunofluorescence imaging of microvasculature surrounding gels. (E-F) Enlarged view of microvascular network in the region of a secondary-to-tertiary venular branch point near the hydrogel (scale bar = 500 μ m) (G) Analysis of 4mm-diameter circular ROI circumscribing each gel region (shown in Figure S4) indicates increased density of microvessels near aHep^N-SDF hydrogels compared to internal control in all animals (* p <0.05 by paired t -test, n =3, lines connect paired analysis of internal control and experimental gels in each animal).